

Article

Liquid-Solid Interaction to Evaluate Thermal Aging Effects on Carbon Fiber-Reinforced Composites

Poom Narongdej , Jack Hanson , Ehsan Barjasteh  and Sara Moghtadernejad * 

Department of Chemical Engineering, California State University Long Beach, Long Beach, CA 90840, USA; poom.narongdej@csulb.edu (P.N.); jack.hanson@student.csulb.edu (J.H.); ehsan.barjasteh@csulb.edu (E.B.)

* Correspondence: sara.moghtadernejad@csulb.edu; Tel.: +1-(562)-985-7534

Abstract: This study investigated the thermally induced aging effects on a carbon fiber-reinforced composite (CFRP) comprising benzoxazine (BZ) and cycloaliphatic epoxy resin (CER). Herein, we employed various testing methodologies to assess the aging behavior of CFRP samples with differing CER and BZ ratios. Traditional techniques, including aging weight change quantification and qualitative analysis of surface morphology, reveal that higher CER content correlates with increased aging. Additionally, wettability analysis demonstrates that both BZ and BZ-CER composites exhibit heightened hydrophilicity with thermal aging, potentially exacerbating concerns such as icing and surface erosion. Notably, the BZ-CER composite displays greater hydrophilicity compared to the BZ composite, consistent with weight change trends. These findings underscore the utility of surface wettability analysis as a valuable tool for monitoring thermo-oxidative aging in polymers and their surface behavior in response to fluid interactions, particularly within high glass transition temperature (T_g) BZ-CER systems utilized in structural composite applications.

Keywords: multiphase interactions; surface wettability; thermal aging



Citation: Narongdej, P.; Hanson, J.; Barjasteh, E.; Moghtadernejad, S. Liquid-Solid Interaction to Evaluate Thermal Aging Effects on Carbon Fiber-Reinforced Composites. *Fluids* **2024**, *9*, 100. <https://doi.org/10.3390/fluids9050100>

Academic Editors: Markus Klein, Tomoaki Kunugi and Yukihiko Yonemoto

Received: 30 March 2024

Revised: 17 April 2024

Accepted: 20 April 2024

Published: 23 April 2024



Copyright: © 2024 by the authors. Licensee MDPI, Basel, Switzerland. This article is an open access article distributed under the terms and conditions of the Creative Commons Attribution (CC BY) license (<https://creativecommons.org/licenses/by/4.0/>).

1. Introduction

Carbon fiber-reinforced composites (CFRPs) are commonly utilized in aerospace and automotive applications due to their low density, among other desired properties [1–3]. Thermosetting resins, specifically benzoxazine (BZ), are often used in the manufacturing of CFRPs due to specific characteristics such as thermal resistance and near-zero volume changes [4]. Recent studies have shown the benefits of copolymerizing BZ with cycloaliphatic epoxy resin (CER) by mitigating their individual undesirable properties, resulting in a resin system with low viscosity that is desirable for advanced composite processing; the resulting composition garnishes an increase of up to 40% in the glass transition temperature and a cross-linked density that can be suitable in high-temperature aerospace applications [4,5]. Weight loss, surface cracking, and surface morphology changes often arise from thermo-oxidative degradation of such copolymers at high temperatures, making the aforementioned properties significant for use in industry [4,6]. Monitoring the thermo-oxidative aging of polymers is conventionally conducted by measuring the change in the weight of structures over time. Using the entire structure for weight measurement is often not practical; instead, small specimens are typically used to carry out accelerated aging experiments. Since the measured weight change results from both the thermo-oxidative aging of the surface and thermal degradation of the bulk of polymers, the weight change alone cannot exactly represent the thermo-oxidative-induced changes to the surface [7]. Regardless, this measurement system can be used in a standardized fashion to effectively compare differing polymer materials. Alternative evaluation methods often consist of mechanical and thermal characterizations over time, but these methods are often not economical and require the destruction of the materials [3].

Another method to measure degradation over time is surface wettability science, which has shown to be an efficient and inexpensive method to monitor and understand the effects

of thermo-oxidative aging in copolymer substrates [4]. In real-life applications, CFRPs are often exposed to high temperatures and moisture, as well as the impact of water droplets in the form of rain [8–10]. The static and dynamic interactions of water droplets upon the surface of industry materials can cause hydrolysis, erosion, and icing, ultimately leading to the acceleration of catastrophic failure over time [11–13]. Often, large droplets can create small satellite droplets upon impact when combined with high water-hammer pressures, leading to severe erosion, degradation, and eventual destruction of surfaces [11]. Upon impact, droplets may rebound off, deposit on, or break up upon a surface; this resulting behavior is influenced by surface characteristics, liquid properties, impact angle, and impact velocity [14–19]. Upon landing of droplets on the surface of structural components such as aircraft and wind turbine blades [16,17], the droplets deform into narrow liquid streams, known as rivulets [18–21], which then form ice in colder environments.

To improve the aforementioned structures' ability to resist corrosion and icing, understanding droplet impact dynamics is essential [22–24]. Droplet impact tests under static and dynamic conditions are conducted in this work to monitor such performance. In our previous investigation [4], we analyzed the behavior of copolymers under thermo-oxidative aging conditions using surface characterization techniques. BZ homopolymer and BZ-CER copolymer samples underwent thermal aging in an air-circulating oven at controlled temperatures of 180 °C and 200 °C for various durations. Our findings demonstrated that the extent of degradation increased with prolonged aging time and higher temperatures. Notably, the BZ-CER copolymer exhibited a more substantial degree of thermo-oxidative degradation compared to the benzoxazine homopolymer. Furthermore, results from surface analysis measurements, such as contact angle, paralleled trends observed in traditional aging experiments, including weight change. To validate real-world applicability, it is imperative to utilize both BZ homopolymers and BZ-CER copolymers in CFRP fabrication and investigate their properties alongside surface wettability.

In this study, we aimed to build upon prior research [4] by exploring the application of surface wettability analysis as a novel approach to monitor the thermal oxidation of CFRPs. Additionally, we investigated the impact of water droplets on thermally aged samples, particularly in terms of icing and surface erosions. CFRP samples fabricated with BZ and BZ-CER copolymer were subjected to high temperatures of 180 °C and 200 °C for various durations, up to 12 weeks. Surface wettability and liquid mobility were assessed through static contact angle and contact angle hysteresis measurements on the aged samples. Furthermore, to simulate real-world scenarios, droplet impact tests were conducted on both static and moving samples (with a velocity of $V_s = 5$ m/s) to better understand water droplet interactions with the aged surface.

2. Materials and Methods

2.1. Composite Fabrication and Thermal Aging

The composite samples were prepared via a vacuum-assisted resin transfer molding (VARTM) process, consisting of eight unidirectional (UD) dry carbon fiber plies with a dimension of 30.48 cm by 30.48 cm, as shown in Figure 1. The layup was arranged in one direction and was infused at 110 °C with a resin mixture of benzoxazine-A-based resin (BZ) (Huntsman Corp., Woodlands, TX, USA) and 131–143 g/eq cycloaliphatic epoxy resin (CER) (Lindau Chemicals, Columbia, SC, USA) at various BZ:CER weight ratios (wt%) of 100:0, 87.5:12.5, 75:25, and 62.5:37.5. The composite panel was then cured at 180 °C for 2 h, 200 °C for 2 h, and 220 °C for 2 h. Once the curing process was completed, the cured panel was cut into 2.54 cm by 2.54 cm square samples and aged in programmable ovens at temperatures of 180 °C and 200 °C for periods of 2, 4, 8, and 12 weeks, producing 32 unique samples for analysis.

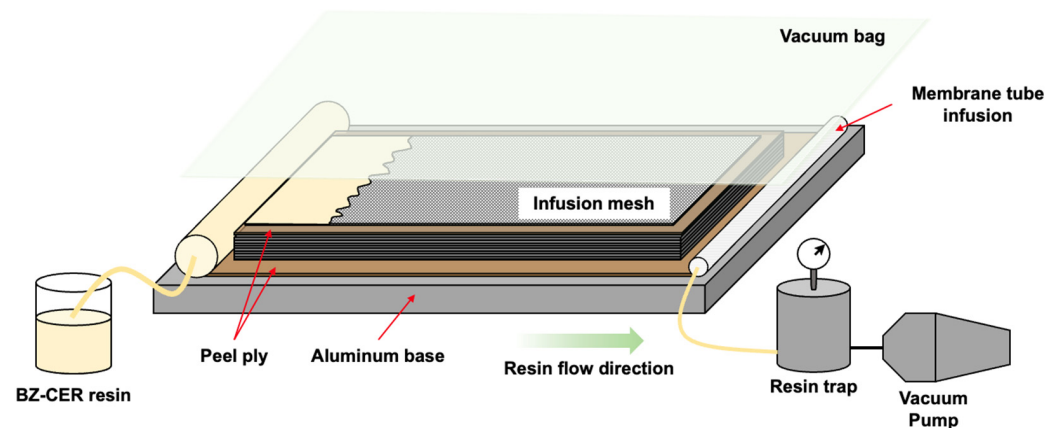


Figure 1. Composite fabrication process via a vacuum-assisted resin transfer molding (VARTM) method.

2.2. Weight Change and Optical Microscopy

Prior to weighing the 32 samples after the aging process, each sample was placed in a desiccator to ensure that any moisture absorbed into the samples had been purged. A microbalance was used to weigh each sample with a precision of 10^{-5} g, and weight change was then calculated from the equation:

$$W_t(\%) = \left(\frac{w_t}{w_0} \right) \times 100\% \quad (1)$$

where $W_t(\%)$ represents the relative weight change percentage of the sample, w_t represents the weight of the sample after time interval t , and w_0 represents the initial weight of the sample. A 5X-trinocular boom-stand stereo microscope (AmScope, Irvine, CA, USA) was then utilized to inspect the samples in order to visualize the effects of the thermal aging process on the surface characteristics of the differing CFRPs, particularly those of cracking phenomena, crack initiation, and density, along with the number of cracks, which were analyzed at 5 times magnification for an area of $1 \mu\text{m}^2$.

2.3. Characterization of Flexural Properties

The flexural strength was characterized in accordance with ASTM D790 via a three-point bending test. The tested samples were cut with the dimensions of 12.7 mm (in width) \times 114.3 mm (in length) \times 2.55 mm (in thickness). A universal testing machine (AGS-X, Shimadzu, Kyoto City, Japan) with a 10 kN load was used to conduct this test. The span length was fixed at 81.6 mm, and the crosshead motion rate was set at 1.27 mm/min. Five samples were conducted for each sample set, and the average value was reported.

2.4. Characterization of Contact Angle, Contact Angle Hysteresis, and Droplet Impact

A unique experimental apparatus was designed in-house to capture contact angle, contact angle hysteresis, and impact phenomena (Figure 2). The setup was composed of a 0.3 m stroke pneumatic air cylinder (Parker-Hannifin, Cleveland, OH, USA) with a custom-machined sample holder fastened to the piston rod for attaching the experimental CFRP samples. This pneumatic cylinder was secured upon a wooden block to ensure no countermovement occurred upon release and fitted with quick exhaust valves (Parker Legris, Cleveland, OH, USA) to increase rod speed per PSIG. To actuate the cylinder, a 5-way solenoid valve (U.S. Solid, Cleveland, OH, USA) was integrated between a 6-gallon air compressor (DeWalt, Baltimore, MD, USA) and the cylinder inlet. This solenoid valve was activated by use of an Arduino Uno (Arduino, Somerville, MA, USA) microcontroller, which was programmed to activate the solenoid valve when it received a specific analog input from an active infrared sensor due to a droplet passing by. Droplets were dispensed from a sterilized syringe with a 0.3 mm needle and all data were captured at 6400 FPS by a Photron FASTCAM (Photron, Tokyo, Japan) with the use of the shadowgraphy technique.

This shadowgraphy method required an LED light with a light diffuser (GS Vitec GmbH, Hesse, Germany), which illuminated the subject area being captured.

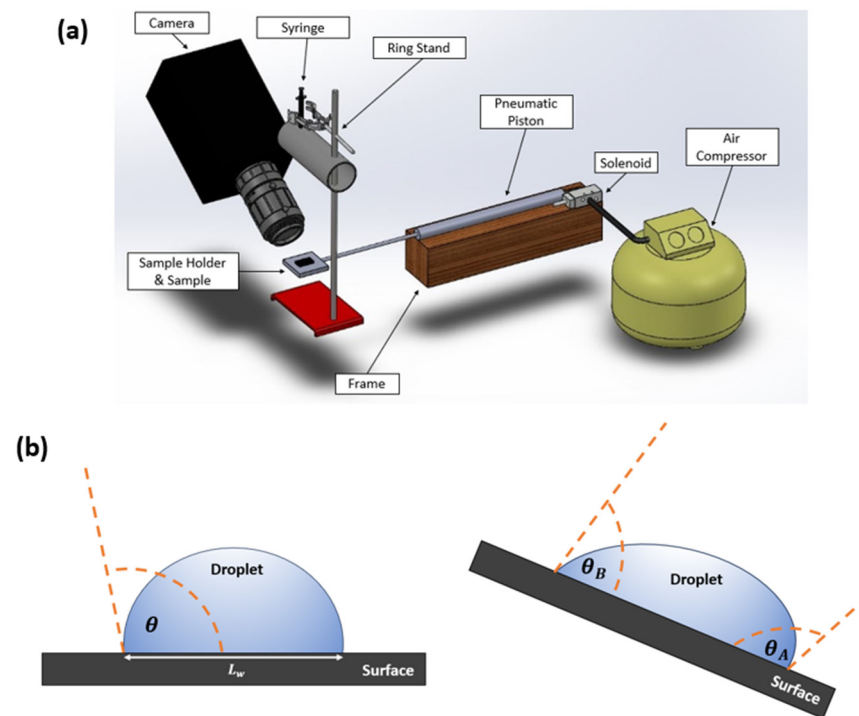


Figure 2. (a) Three-dimensional illustration of the experimental setup for droplet impact trials. (b) Schematic of (left) contact angle and wetting length (L_w) and (right) contact angle hysteresis.

Contact angle (CA) was measured using a sessile droplet method on the static condition. Initially, a liquid droplet was deposited from the syringe onto the surface of the CFRP samples. The high-speed camera captured an image of the sessile droplet on the sample immediately after placement. The angle between the droplet and surface was then measured as the static contact angle, which describes surface wettability. Contact angle hysteresis (CAH) is a parameter indicating liquid mobility on the surface. To measure hysteresis, the surface was tilted until the droplet was about to slide, and this process was recorded with the high-speed camera. Hysteresis was defined by the difference between the advancing angle (θ_A) and the receding angle (θ_B), denoted as $\Delta\theta = \theta_A - \theta_B$ (see Figure 2b). A smaller value of hysteresis ($\Delta\theta$) indicates easier movement of the droplet on the surface. Note that both CA and CAH of the droplets were recorded by post-processing via Photron FASTCAM Viewer 4 [PFV4] software.

In the stationary and moving impact, the droplet was dispensed from a ring stand at a height of 24 cm. In the stationary impact, no actuation of the cylinder was involved, and thus the droplet was able to be dispensed and fall vertically onto the CFRP. In the moving impact, the cylinder was actuated with 100 PSIG to gain a velocity of 5 m/s, and the droplet was timed through programmed delay in the code to have solenoid activation and subsequent rod extension align with the time, in which the droplet would reach the height of the moving surface. These trials were post-processed in PFV4 to capture the wetting length over time, L_w , beginning at the moment of impact ($t = 0$), and ending upon the observation of the droplet returning to equilibrium or breaking into multiple bodies.

3. Results and Discussions

3.1. Weight Change

Figure 3 shows the evolution of weight loss over aging time for specimens with varying proportions of BZ and CER. As shown in Figure 3a, all samples exhibited a decrease in weight during the first two weeks of aging at 180 °C, with an average of 0.03% loss relative

to their initial weight. Subsequently, the weights of the samples were observed to stabilize with their weight loss less than 0.01% from week 0 through 12. The observed weight change in both homopolymer (BZ) and copolymer (BZ-CER) composites aligns with findings from our prior research [4], attributed to thermal oxidation at the matrix’s surface and polymer degradation due to elevated temperatures [25]. This process led to microcrack formation on the matrix surface, facilitating oxygen penetration and resulting in intensified weight change with prolonged exposure [4]. Furthermore, the higher CER content in the BZ-CER composite was observed to increase susceptibility to weight variation when subjected to thermal aging, indicating greater vulnerability. Conversely, higher BZ content suggests enhanced resistance to such effects. This observation highlights the finding in our previous study [4], wherein copolymerization of BZ with CER diminished the thermal stability of the BZ system.

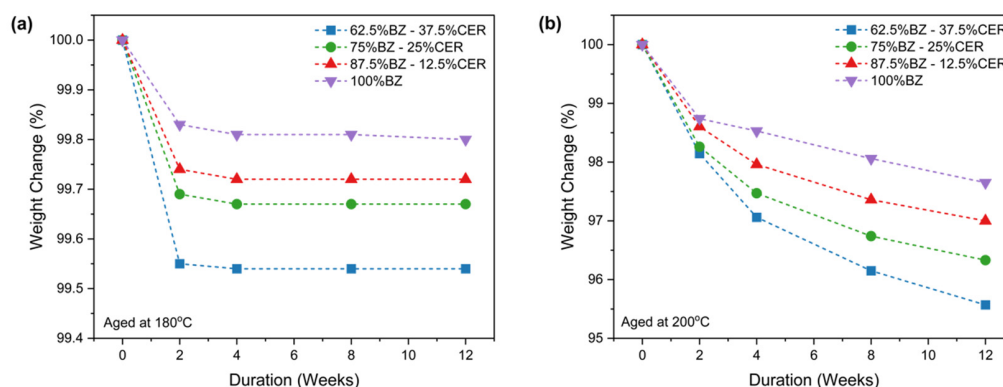


Figure 3. Effects of aging duration up to 12 weeks on weight change at (a) 180 °C and (b) 200 °C on samples with differing BZ to CER ratios. Experimental uncertainty is within 5%.

Figure 3b demonstrates the weight changes in all samples subjected to thermal aging at 200 °C. Notably, a significant weight loss becomes increasingly pronounced over time for both homopolymers and copolymers compared to aging at 180 °C. The rate of weight change intensifies, with samples losing nearly 3% of their weight over the 12-week aging period. This observation underscores the heightened susceptibility of samples to weight fluctuations as temperature rises, indicative of thermal aging degradation. This finding aligns with our prior study [4], where the extent of microcracking on the surface of samples exposed at 200 °C was more severe and deeper than that on samples exposed at 180 °C. Regarding the weight change ratio, the data at 200 °C mirror trends observed at 180 °C, with samples containing 100% BZ to CER being the least affected and those with a 62.5:32.5 ratio experiencing the most substantial changes. These results emphasize that CER demonstrates a stronger tendency for thermal-oxidative degradation in comparison to BZ.

3.2. Flexural Properties

Figure 4 presents a comparative analysis of the flexural strength of specimens containing varying proportions of BZ and CER, subjected to aging at temperatures of 180 °C and 200 °C. At 180 °C, a slight reduction in flexural strength was found. By the 12th week, flexural strength decreased by 2.18%, 4.17%, 2.42%, and 3.22% for composites with 0 wt%, 12.5 wt%, 25 wt%, and 37.5 wt% CER addition, respectively. However, at 200 °C, a substantial and more pronounced decrease in flexural strength was observed. The values decreased by 12.43%, 16.82%, 16.57%, and 14.84% for composites with 0 wt%, 12.5 wt%, 25 wt%, and 37.5 wt% CER addition, respectively. Among the tested BZ-CER ratios, specimens with pure homopolymer (100% BZ) exhibited the most significant reduction in flexural strength. This decline at 200 °C is attributed to degradation in functionality and structural changes in both BZ and CER resins at the microscopic level, along with increased presence of voids and cracks in the matrix phase induced by stress gradients from oxidized matrix shrinkage at high temperatures [26–29].

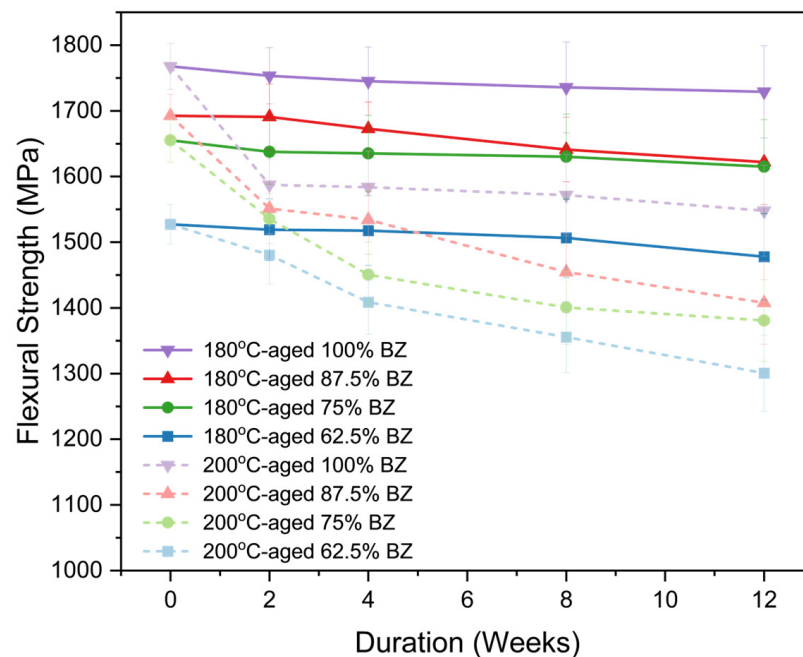


Figure 4. Flexural strength of samples with various BZ-CER contents aged at 180 °C and 200 °C for 12 weeks. Experimental uncertainty is within 5%.

Moreover, considering the effect of CER content, increasing CER concentration decreases the flexural strength of the composite panel. Our prior study [4] found that adding CER to BZ-CER composites led to a degradation in thermal stability due to a significantly higher reduction in alkoxy, sp^3 -aliphatic, and hydroxyl functional groups compared to pure BZ composites, aligning with the observed flexural properties. Additionally, it should be noted that the flexural behaviors of both pure BZ and BZ-CER composites correspond with the observed weight loss.

3.3. Microscopic Analysis

Figure 5 shows microscopic images of the surface conditions of samples aged for 4, 8, and 12 weeks of varying BZ-CER ratios as compared to unaged samples. When aged at 180 °C, regardless of the BZ and CER ratios, the specimen surfaces show minimal signs of deterioration. However, upon elevating the aging temperature to 200 °C, surface degradation becomes more visible, with increased fiber exposure during prolonged aging, as highlighted by the yellow arrows in Figure 5a.

However, this degradation diminishes as the BZ content increases, resulting in reduced matrix cracking and diminished fiber exposure, as denoted by the green and red arrows in Figures 5b and 5c, respectively. The composite consisting of pure BZ (100 wt% BZ) in Figure 5d exhibits excellent resistance to thermal aging, with no noticeable fiber exposure and only minor matrix cracking, as indicated by the yellow arrows. This surface morphology underscores the correlation between increasing weight loss with prolonged aging at higher temperatures and the milder surface cracking associated with higher BZ content.

3.4. Static Contact Angle

The contact angle results provide quantification of wettability changes induced by thermal aging. Figure 6 illustrates the change in contact angle of sessile droplets on the composite sample surfaces, emphasizing how this angle evolves with increasing thermal aging time. Static contact angle measurements offer direct insight into a surface's wettability, reflecting its propensity to interact with water. Both BZ-CER and BZ samples are shown with plot overlays at different aging temperatures (180 °C and 200 °C).

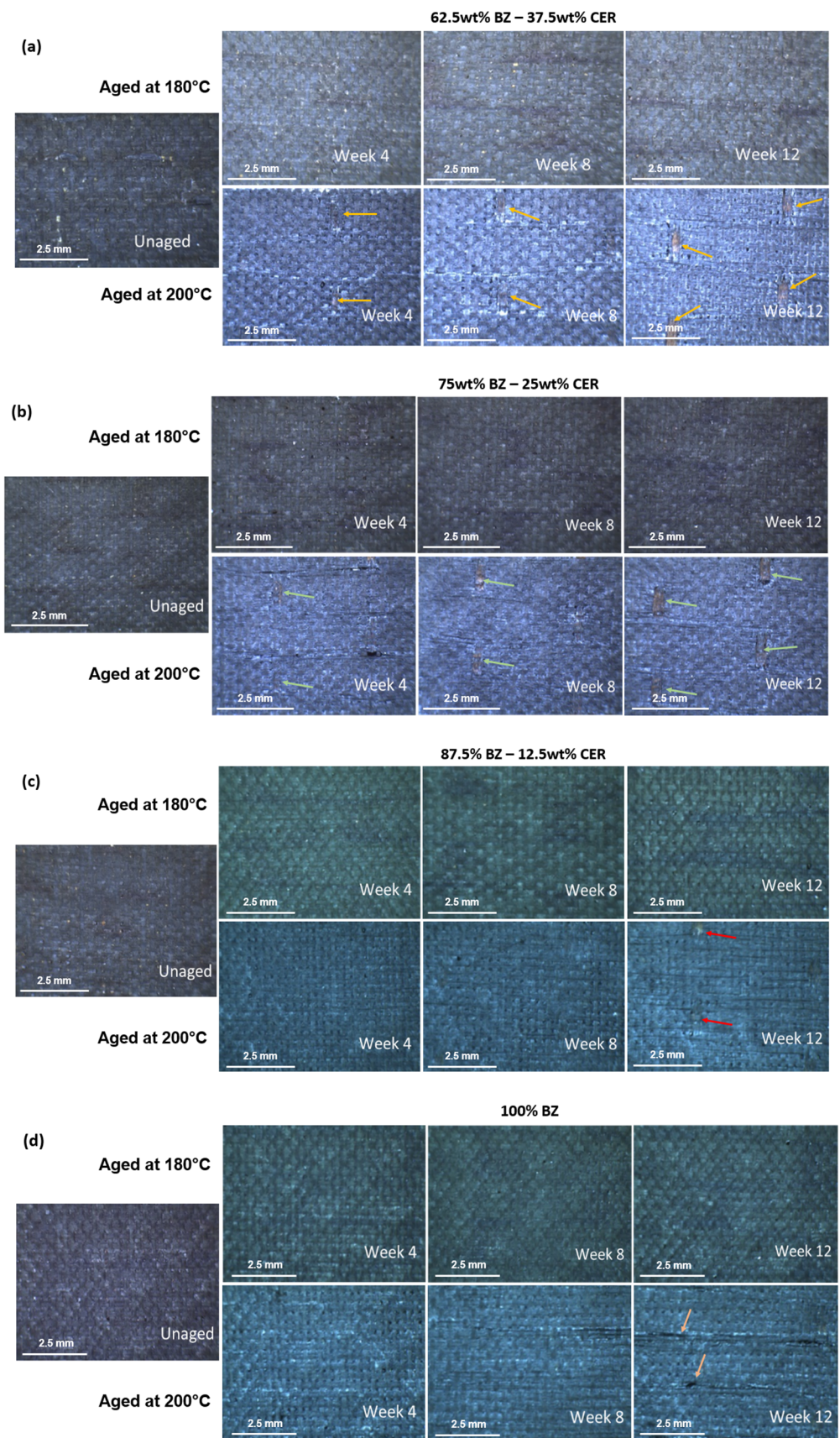


Figure 5. Surface morphology of different BZ and CER ratios aged at 180 °C and 200 °C for 12 weeks: (a) 62.5 wt% BZ–37.5 wt% CER, (b) 75 wt% BZ–25 wt%, (c) 87.5 wt% BZ–12.5 wt% CER, and (d) 100 wt% BZ.

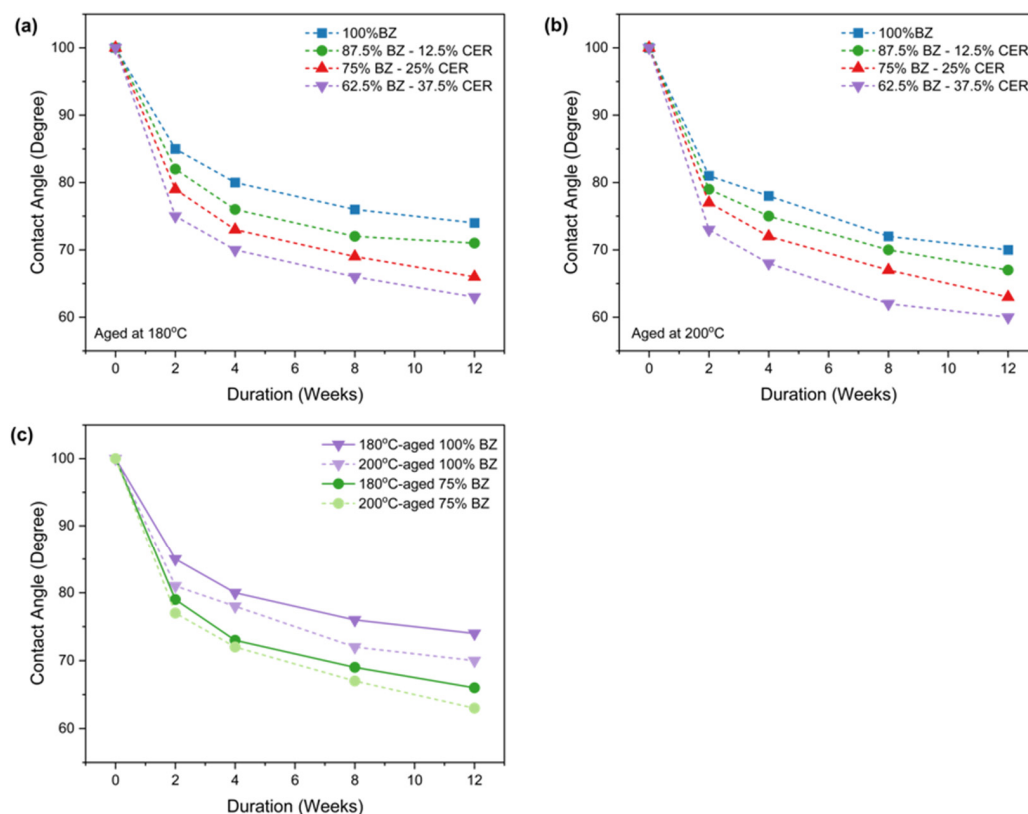


Figure 6. Contact angle as a function of aging duration on pure BZ and various BZ-CER ratios aged at (a) 180 °C and (b) 200 °C. (c) Comparison of contact angle as a function of aging duration between 100 wt% BZ and 75 wt% BZ by weight aged at 180 °C and 200 °C.

Observations show that both homopolymer (BZ) and copolymer (BZ-CER) composites exhibit a decrease in contact angle with prolonged aging duration. As shown in Figure 6a, the change in contact angle values of BZ-CER samples surpasses those of BZ when aged at 180 °C. This discrepancy is primarily attributed to the presence of greater intermolecular hydrogen bonding within the copolymer samples, subsequently enhancing surface energy [4]. Specifically, within the initial 2 weeks of exposure, the contact angle of homopolymer BZ decreases by nearly 15%, gradually declining by 26% after 12 weeks of aging. In comparison, the change in contact angles of BZ-CER copolymers diminishes by 18%, 21%, and 25% for samples containing 12.5 wt%, 25 wt%, and 37.5 wt% CER, respectively, within the initial 2 weeks of aging. Subsequently, the contact angles of BZ-CER copolymers further decrease by 29%, 34%, and 37% for samples with 12.5 wt%, 25 wt%, and 37.5 wt% CER, respectively, after 12 weeks of aging.

Figure 6b illustrates the change in contact angle values of both BZ homopolymer and BZ-CER copolymer composites aged at 200 °C for 12 weeks. It was observed that after 2 weeks of aging, the contact angles of all samples decreased by 19%, 21%, 23%, and 27% for samples with 0 wt%, 12.5 wt%, 25 wt%, and 37.5 wt% CER, respectively. By week 12, the contact angles further reduced by 30%, 33%, 37%, and 40% for samples with 0 wt%, 12.5 wt%, 25 wt%, and 37.5 wt% CER, respectively. These decreases were more pronounced than those observed in samples aged at 180 °C. The greater decrease in contact angle values of samples aged at 200 °C compared to 180 °C can be attributed to more severe thermal oxidation at higher exposure temperatures [4].

In Figure 6c, a comparison of contact angles between composites containing 100 wt% BZ and 75 wt% BZ–25 wt% CER is depicted. It is notable that the addition of CER to the BZ system resulted in a greater reduction in contact angle with increasing aging duration at both 180 °C and 200 °C. This observation suggests that the higher CER content in the BZ system renders the composite surface less hydrophobic due to the inherently hydrophilic

nature of epoxy [30,31]. Moreover, this trend towards increased hydrophilicity intensifies as the composites are exposed to higher temperatures over time.

3.5. Contact Angle Hysteresis

In this work, the mobility of droplets over the analyzed composite surfaces was characterized through contact angle hysteresis. Figure 7 illustrates an upward trend in contact angle hysteresis with increasing aging time for all samples, indicating that thermal aging led to the creation of surfaces with reduced droplet mobility. After 12 weeks of aging at 180 °C, the contact angle hysteresis in the homopolymer BZ composite increased by 85%, while for copolymer BZ-CER composites with 12.5%, 25%, and 37.5% CER, it increased by 88.89%, 93.75%, and 86.67%, respectively, as shown in Figure 7a.

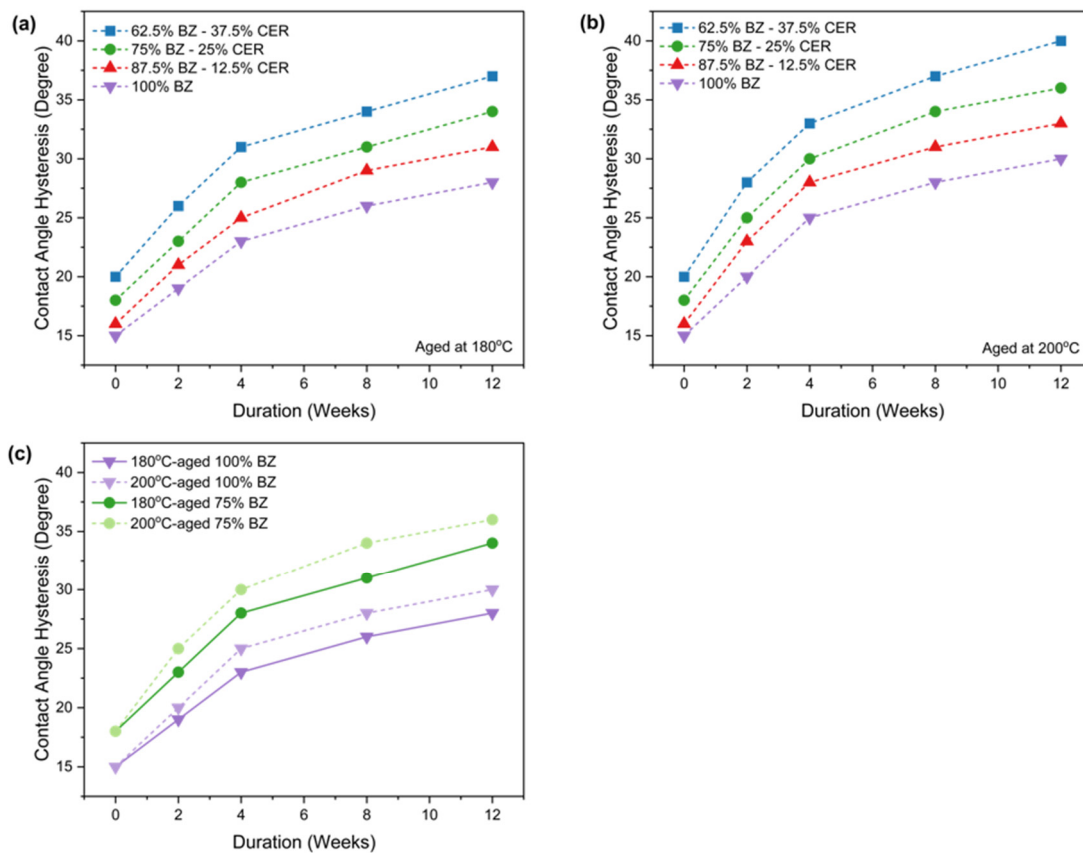


Figure 7. Contact angle hysteresis as a function of aging duration on pure BZ and various BZ-CER ratios aged at (a) 180 °C and (b) 200 °C. (c) Comparison of contact angle hysteresis as a function of aging duration between 100 wt% BZ and 75 wt% BZ by weight aged at 180 °C and 200 °C.

When the composites were exposed to higher aging temperatures at 200 °C, the contact angle hysteresis of each sample increased, as depicted in Figure 7b. Figure 7c presents a comparison between BZ and BZ-CER composites aged at 180 °C and 200 °C, revealing that BZ composites had smaller values of contact angle hysteresis compared to BZ-CER composites. This aligns with the trend identified in our previous study [4] and confirms that the liquid mobility on the copolymer composites was lower than that of the homopolymer composites.

3.6. Static Droplet Impact

The commonly used commercial composite with a ratio of 75 wt% BZ to 25 wt% CER by weight was selected for comparison with pure BZ (100 wt% BZ) regarding their droplet impact behavior under static and dynamic conditions. The droplet geometries were examined on surfaces of specimens aged after two and twelve weeks, respectively,

and their wetting was measured over time. Figure 8a,b illustrate the droplet impact upon stationary samples in terms of wetting length over time on specimens aged after 2 and 12 weeks.

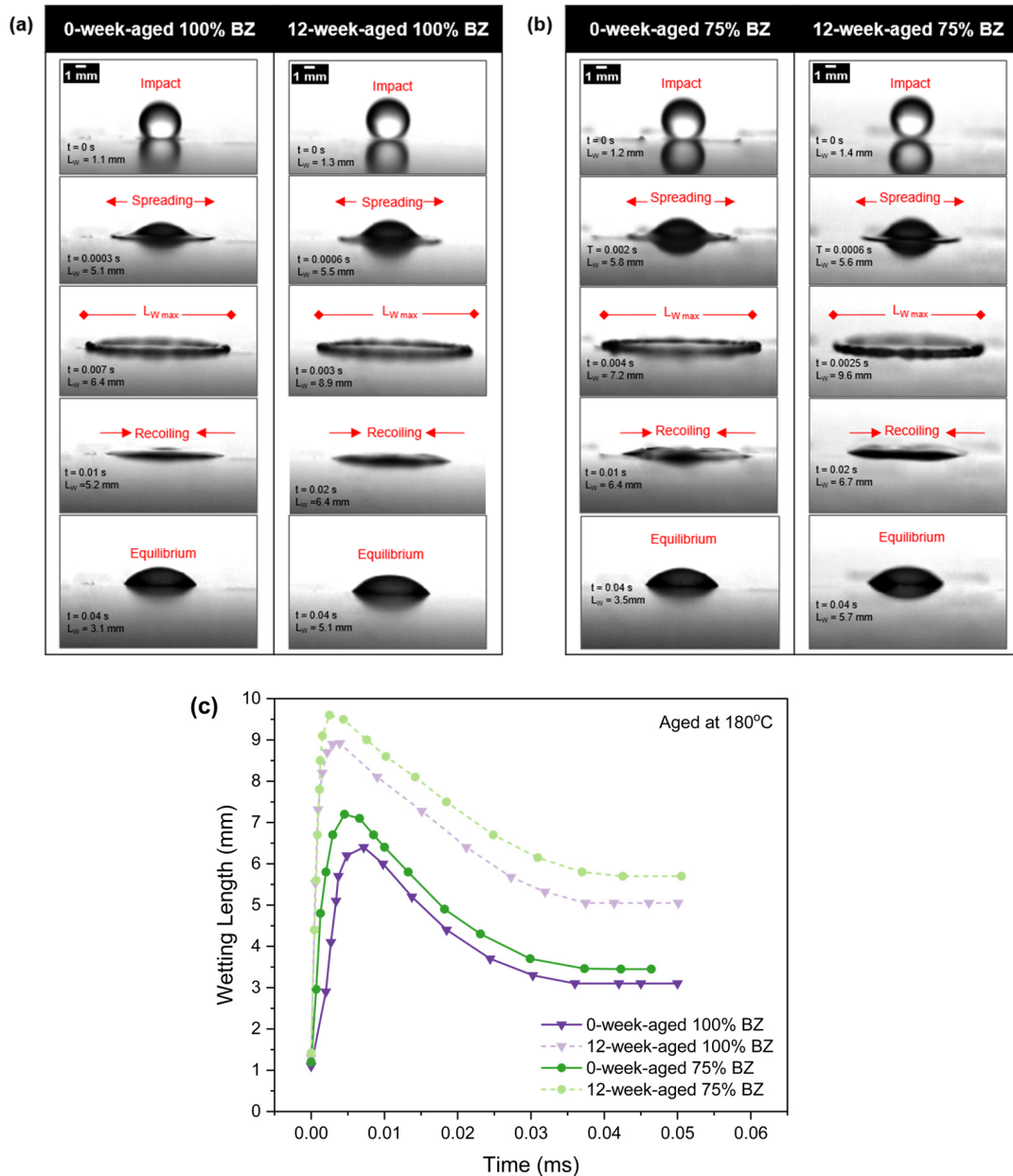


Figure 8. Wetting length versus aging time (at 180 °C) on the stationary samples of BZ and BZ-CER. (a) Droplet impact on a stationary 100% BZ sample at zero and 12-weeks of aging. (b) Droplet impact on a stationary 75% BZ sample at zero and 12-weeks of aging. (c) Wetting length versus time for BZ and BZ-CER samples at zero and 12-weeks of aging.

As depicted in Figure 8a, after the impact, L_w increased, reaching its maximum value of 8.90 mm at 0.003 s for the more hydrophilic aged sample of BZ. Conversely, the time taken for the droplet to reach its L_{wmax} for the unaged sample (more hydrophobic) was higher (0.007 s). Subsequently, the recoiling process commenced until forces reached equilibrium. At this point, the L_w no longer changed, with a value of 5.10 mm for the aged BZ sample and 3.1 mm for the more hydrophobic unaged sample. These results provide insight into how the sample’s surface interacts with the impinging droplet as it spreads and recoils from surface tension forces, shedding light on real-world scenarios.

Figure 8b compares the behaviors of droplets on the copolymer BZ-CER composites. It was observed that the behaviors of both L_w and L_{wmax} of the droplets on the copolymer composites were similar to those of the homopolymer composites, while the difference in L_{wmax} between the aged and unaged samples was more pronounced.

To illustrate the impact phenomena, wetting length versus time for both BZ and BZ-CER samples at unaged and maximum aging duration (12 weeks at 180 °C and 200 °C) is plotted in Figure 8c. Here, the time of 0 ms corresponds to the moment the droplet first contacts the surface, while the final timestamp represents the time at which the droplet returns to equilibrium. Following the droplet impact, as inertia force overcame surface tension forces, L_w increased for all samples until it reached its maximum value, L_{wmax} . The value of L_{wmax} was higher for BZ-CER (9.60 mm) and BZ (8.90 mm) samples aged for 12 weeks compared to the corresponding unaged samples (BZ-CER = 7.20 mm and BZ = 6.40 mm). These results align with our previous analysis of contact angle and contact angle hysteresis, indicating that BZ homopolymer composite was more hydrophobic than the BZ-CER copolymer composite [4]. Furthermore, from the contact angle and contact angle hysteresis analysis, aging resulted in more hydrophilic samples, facilitating easier droplet spreading. Consequently, the liquid reached a greater value of L_{wmax} in a shorter time (the graph shifted to the right-hand side for less hydrophilic samples). After reaching L_{wmax} , the droplet began to recoil, leading to a decrease in L_w . This process concluded when surface tension and inertia forces reached equilibrium, stabilizing L_w at a constant value. Due to the more hydrophilic nature of aged samples compared to unaged ones, the increase in the slope of L_w and its final value were greater for the aged samples. A similar trend was observed for the more hydrophilic BZ-CER samples compared to the BZ sample.

3.7. Dynamic Droplet Impact

To initiate a study of droplet impact on moving BZ surfaces, we recorded the impact incident while the samples were moving axially at a speed of 5 m/s. Remarkably, a similar phenomenon to droplet impact on stationary samples is observable for droplet impact on moving samples, as depicted in Figure 9a,b, which present the same parameters as in the static case.

In the homopolymer BZ composite shown in Figure 9a, following the initial impact on the moving samples, the value of L_w of the BZ samples became 1.10 mm and 1.30 mm for the unaged and 12-week-aged samples, respectively, mirroring the values observed on the stationary surfaces in the previous section. Subsequent to the impact, the spreading phase ensued until a rivulet formed on the surface, leading to a significant increase in the value of L_w . Similarly, comparable behaviors were observed on the surfaces of both unaged and aged copolymer BZ-CER composites, as shown in Figure 9b.

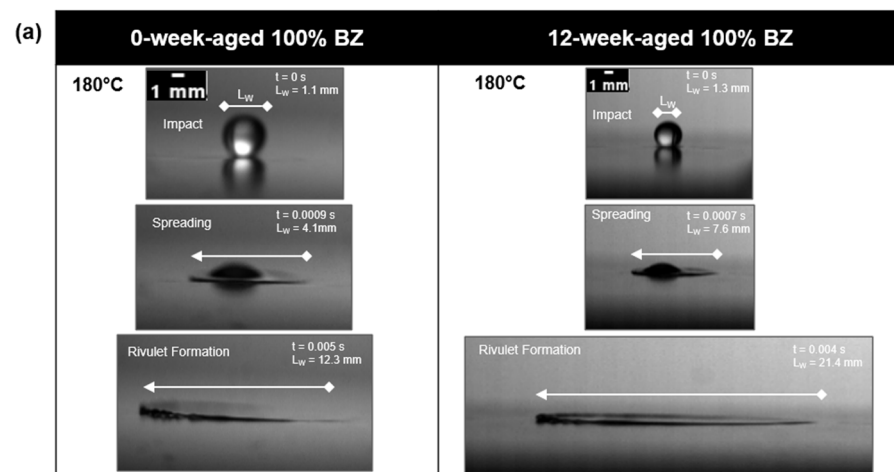


Figure 9. Cont.

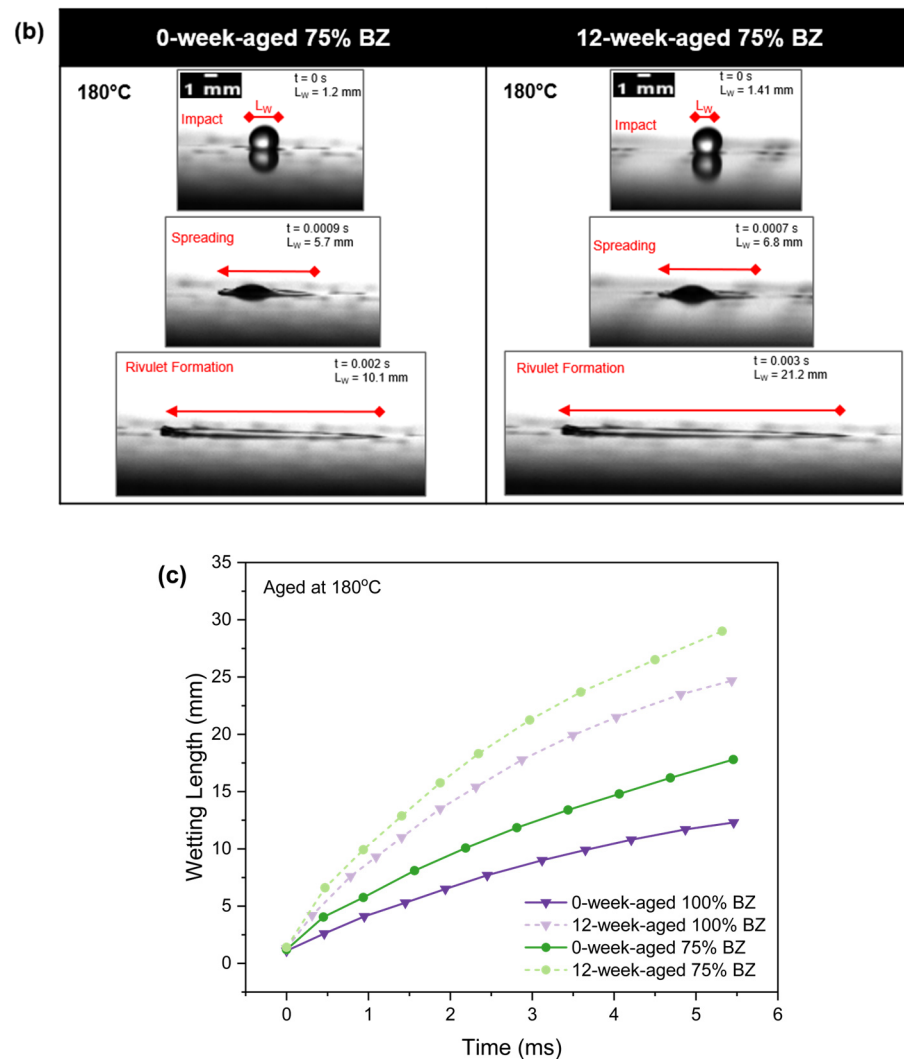


Figure 9. Wetting length versus aging time (at 180 °C) on the moving ($v = 5$ m/s) BZ and BZ-CER samples. (a) Droplet impact on a dynamic 100% BZ sample at zero and 12-weeks of aging. (b) Droplet impacts on a dynamic 75% BZ sample at zero and 12-weeks of aging. (c) Wetting length versus time for BZ and BZ-CER samples at zero and 12-weeks of aging.

Figure 9c presents the variation in L_w versus time for both unaged and aged BZ and BZ-CER composites. The data from samples aged for 12 weeks at 180 °C reveal the maximum change in wetting length. On a more hydrophilic sample, liquid was observed to spread faster, resulting in an increased slope of the value of L_w in the diagram. Consequently, the BZ-CER sample aged for 12 weeks exhibited the greatest values of L_w at each time point, whereas these values were the lowest for the unaged BZ sample. The increase in L_w between unaged and aged BZ and BZ-CER composites was 73.98% and 109.90%, respectively.

4. Conclusions

This study introduced the application of surface wettability analysis as a novel approach to monitor the thermal oxidation of CFRPs. The impact of water droplets on thermally aged samples was investigated, particularly in terms of icing and surface erosion. CFRP samples fabricated with BZ and BZ-CER copolymer were subjected to high temperatures of 180 °C and 200 °C for various durations, up to 12 weeks. The results indicated that at higher temperatures, CFRPs not only experienced a higher and more significant weight loss, but also a significant reduction in flexural properties. This phenomenon was corroborated by the CFRP’s wettability via contact angle and droplet impact characteriza-

tions. It was concluded that high CER content, longer aging durations, and increased aging temperatures led to an enhancement in the hydrophilicity of the composite's surface. These findings underscore the utility of multiphase interactions and surface wettability analysis as valuable tools for monitoring the thermo-oxidative aging of polymers. This discovery emphasizes the importance of understanding and managing aging processes in CFRPs to ensure their long-term performance and reliability across various applications.

Author Contributions: Conceptualization, methodology, investigation, P.N., J.H., E.B. and S.M.; writing—original draft preparation, P.N. and J.H.; writing—review and editing, S.M.; supervision, S.M. All authors have read and agreed to the published version of the manuscript.

Funding: This research received no external funding.

Data Availability Statement: The data that support the findings of this study are available from the corresponding author upon reasonable request.

Acknowledgments: The authors gratefully acknowledge the support of the CSULB Research, Scholarly, and Creative Activity Program. Writing assistance from the AI tool ChatGPT is acknowledged. The ChatGPT writing assistant was used to review and improve the readability of the text. Feedback from ChatGPT was manually reviewed before integrating the suggested sentences into the manuscript.

Conflicts of Interest: The authors declare no conflicts of interest.

References

1. Taylor, T.; Zhang, J.; Yanagimoto, J. Evaluation of a concept out-of-autoclave process for manufacturing carbon fibre reinforced polymer automotive parts. *Procedia CIRP* **2019**, *86*, 162–166. [[CrossRef](#)]
2. Jia, Z.; Li, T.; Chiang, F.; Wang, L. An experimental investigation of the temperature effect on the mechanics of carbon fiber reinforced polymer composites. *Compos. Sci. Technol.* **2018**, *154*, 53–63. [[CrossRef](#)]
3. Zavatta, N.; Rondina, F.; Falaschetti, M.P.; Donati, L. Effect of Thermal Ageing on the Mechanical Strength of Carbon Fibre Reinforced Epoxy Composites. *Polymers* **2021**, *13*, 2006. [[CrossRef](#)]
4. Moghtadernejad, S.; Barjasteh, E.; Johnson, Z.; Stolpe, T.; Banuelos, J. Effect of thermo-oxidative aging on surface characteristics of benzoxazine and epoxy copolymer. *J. Appl. Polym. Sci.* **2021**, *138*, 50211. [[CrossRef](#)]
5. Barjasteh, E.; Gouni, S.; Sutanto, C.; Narongdej, P. Bisphenol-A benzoxazine and cycloaliphatic epoxy copolymer for composite processing by resin infusion. *J. Compos. Mater.* **2019**, *53*, 1777–1790. [[CrossRef](#)]
6. Navarro, C.A.; Kedzie, E.A.; Ma, Y.; Michael, K.H.; Nutt, S.R.; Williams, T.J. Mechanism and catalysis of oxidative degradation of fiber-reinforced epoxy composites. *Top. Catal.* **2018**, *61*, 704–709. [[CrossRef](#)] [[PubMed](#)]
7. Barjasteh, E.; Kar, N.; Nutt, S.R. Effect of filler on thermal aging of composites for next-generation power lines. *Compos. Part A Appl. Sci. Manuf.* **2011**, *42*, 1873–1882. [[CrossRef](#)]
8. Crane, R.I. Droplet deposition in steam turbines. *Proc. Inst. Mech. Eng. Part C J. Mech. Eng. Sci.* **2004**, *218*, 859–870. [[CrossRef](#)]
9. Sun, L.; Zheng, Q.; Luo, M.; Li, Y.; Bhargava, R. On the Behavior of Water Droplets When Moving onto Blade Surface in a Wet Compression Transonic Compressor. *J. Eng. Gas Turbines Power* **2011**, *133*, 082001. [[CrossRef](#)]
10. Zhou, Q.; Li, N.; Chen, X.; Xu, T.; Hui, S.; Zhang, D. Analysis of water drop erosion on turbine blades based on a nonlinear liquid–solid impact model. *Int. J. Impact Eng.* **2009**, *36*, 1156–1171. [[CrossRef](#)]
11. Dunn, T.A.; Loth, E.; Bragg, M.B. Computational Investigation of Simulated Large-Droplet Ice Shapes on Airfoil Aerodynamics. *J. Aircr.* **1999**, *36*, 836–843. [[CrossRef](#)]
12. Cebeci, T.; Kafyeke, F. Aircraft Icing. *Annu. Rev. Fluid Mech.* **2003**, *35*, 11–21. [[CrossRef](#)]
13. Thomas, S.K.; Cassoni, R.P.; MacArthur, C.D. Aircraft anti-icing and de-icing techniques and modeling. *J. Aircr.* **1996**, *33*, 841–854. [[CrossRef](#)]
14. Antonini, C.; Carmona, F.J.; Pierce, E.; Marengo, M.; Amirfazli, A. General Methodology for Evaluating the Adhesion Force of Drops and Bubbles on Solid Surfaces. *Langmuir* **2009**, *25*, 6143–6154. [[CrossRef](#)] [[PubMed](#)]
15. Schleizer, A.D.; Bonnecaze, R.T. Displacement of a two-dimensional immiscible droplet adhering to a wall in shear and pressure-driven flows. *J. Fluid Mech.* **1999**, *383*, 29–54. [[CrossRef](#)]
16. Li, J.Y.; Yuan, X.F.; Han, Q.; Xi, G. Impact patterns and temporal evolutions of water drops impinging on a rotating disc. *Proc. Inst. Mech. Eng. Part C J. Mech. Eng. Sci.* **2011**, *226*, 956–967. [[CrossRef](#)]
17. Hung, Y.L.; Wang, M.J.; Huang, J.W.; Lin, S.Y. A study on the impact velocity and drop size for the occurrence of entrapped air bubbles-Water on parafilm. *Exp. Therm. Fluid Sci.* **2013**, *48*, 102–109. [[CrossRef](#)]
18. Yarin, A.L. Drop impact dynamics: Splashing, spreading, receding, bouncing. ... *Annu. Rev. Fluid Mech.* **2006**, *38*, 159–192. [[CrossRef](#)]

19. Khojasteh, D.; Kazerooni, M.; Salarian, S.; Kamali, R. Droplet impact on superhydrophobic surfaces: A review of recent developments. *J. Ind. Eng. Chem.* **2016**, *42*, 1–14. [[CrossRef](#)]
20. Holl, M.; Patek, Z.; Smrcek, L. Wind tunnel testing of performance degradation of ice contaminated airfoils. *ICAS Tech. Paper* **2000**, *3*, 2000.
21. Li, R.; Ashgriz, N.; Chandra, S.; Andrews, J.R.; Drappel, S. Coalescence of two droplets impacting a solid surface. *Exp. Fluids* **2010**, *48*, 1025–1035. [[CrossRef](#)]
22. Cao, L.; Jones, A.K.; Sikka, V.K.; Wu, J.; Gao, D. Anti-Icing Superhydrophobic Coatings. *Langmuir* **2009**, *25*, 12444–12448. [[CrossRef](#)]
23. Chen, X.; Wang, P.; Zhang, D.; Ou, J. Rational fabrication of superhydrophobic surfaces with coalescence-induced droplet jumping behavior for atmospheric corrosion protection. *Chem. Eng. J.* **2021**, *428*, 132029. [[CrossRef](#)]
24. Pan, R.; Zhang, H.; Zhong, M. Triple-Scale Superhydrophobic Surface with Excellent Anti-Icing and Icephobic Performance via Ultrafast Laser Hybrid Fabrication. *ACS Appl. Mater. Interfaces* **2021**, *13*, 1743–1753. [[CrossRef](#)]
25. Barjasteh, E.; Bosze, E.J.; Tsai, Y.I.; Nutt, S.R. Thermal aging of fiberglass/carbon-fiber hybrid composites. *Compos.-A Appl. Sci. Manuf.* **2009**, *40*, 2038–2045. [[CrossRef](#)]
26. Bhargava, R.; Wang, S.Q.; Koenig, J.L. FTIR microspectroscopy of polymeric systems. *Adv. Polym. Sci.* **2003**, *163*, 137–191.
27. Ernault, E.; Richaud, E.; Fayolle, B. Thermal oxidation of epoxies: Influence of diamine hardener. *Polym. Degrad. Stab.* **2016**, *134*, 76–86. [[CrossRef](#)]
28. Minervino, M.; Gigliotti, M.; Lafarie-Frenot, M.C.; Grandidier, J.C. The effect of thermo-oxidation on the mechanical behaviour of polymer epoxy materials. *Polym. Test.* **2013**, *32*, 1020–1028. [[CrossRef](#)]
29. Chernykh, A.; Agag, T.; Ishida, H. Synthesis of linear polymers containing benzoxazine moieties in the main chain with high molecular design versatility via click reaction. *Polymer* **2009**, *50*, 382–390. [[CrossRef](#)]
30. Zhou, C.; Xin, Z. Polybenzoxazine-based coatings for corrosion protection. *Adv. Emerg. Polybenzoxazine Sci. Technol.* **2017**, 1003–1017. [[CrossRef](#)]
31. Zhang, S.Y.; Ding, Y.F.; Li, S.J.; Luo, X.W.; Zhou, W.F. Effect of polymeric structure on the corrosion protection of epoxy coatings. *Corros. Sci.* **2002**, *44*, 861–869. [[CrossRef](#)]

Disclaimer/Publisher’s Note: The statements, opinions and data contained in all publications are solely those of the individual author(s) and contributor(s) and not of MDPI and/or the editor(s). MDPI and/or the editor(s) disclaim responsibility for any injury to people or property resulting from any ideas, methods, instructions or products referred to in the content.